



DESIGN NOTE: THERMAL DESIGN CONCEPT

Original Author: John Rayner

Latest Revision: John Rayner



NASA Infrared Telescope Facility
Institute for Astronomy
University of Hawaii

Revision History

Revision No.	Author & Date	Approval & Date	Description
Revision 1	John Rayner 10 December 2010		First release
Revision 2	John Rayner 29 January 2013		Second release



Contents

1 INTRODUCTION 3
1.1 Purpose..... 3
1.2 Applicable and Reference Documents 3

2 THERMAL DESIGN REQUIREMENTS..... 3
2.1 Fundamental requirements 3
2.2 Practical requirements..... 8
2.3 Summary of high-level thermal design requirements 8

3 CRYOSTAT CONCEPT 9
3.1 Design options..... 9
3.2 SpeX cryostat..... 9
3.2.1 Description 9
3.2.2 Thermal analysis methods..... 12
3.2.3 Cryostat thermal model..... 19
3.2.4 Cryostat performance..... 25
3.3 Proposed iSHELL concept..... 28
3.3.1 Thermal design options 28
3.3.2 Proposed thermal design..... 29

1 INTRODUCTION

1.1 Purpose

This document describes the thermal design concept of the infrared high-resolution immersion grating spectrograph for IRTF (iSHELL). It serves a number of purposes. It links the science requirements to the top-level requirements of the thermal design, presents thermal design options, and considers the IRTF's experience with SpeX which has very similar thermal requirements to iSHELL. From these considerations a thermal design concept is developed and presented. This document is intended for use by the engineers developing detailed designs for the cryostat and internal support structures, optics and optical baffles, mechanisms, and temperature regulation systems.

1.2 Applicable and Reference Documents

Reference	Document Title	Document Number	Issue
AD2	Science Requirements Document	iSHELL-SPEC-00002-0001	1.0
AD3	Controller Requirements Document	iSHELL-SPEC-00003-0001	1.0
AD4	Functional Performance Requirements Document	iSHELL-SPEC-00004-0001	1.0

2 THERMAL DESIGN REQUIREMENTS

2.1 Fundamental requirements

The science case requires that iSHELL must meet certain sensitivity requirements (SR-2 Sensitivity). For optimum sensitivity the detector array must be operated at a temperature at which dark current is minimized while at the same time not adversely affecting read noise and quantum efficiency (QE). For the H2RG array used in the spectrograph this temperature is about 38 K, at which temperature the dark current lies in the range 0.01 (leakage) to 0.1 electrons/sec (persistence), and depends upon the performance of the individual array used (leakage) and prior illumination (persistence and residual image effects). Figure 1 plots the signal from the dominant background sources, namely the sky, telescope, scattered light from the moon, and internal thermal background from the instrument enclosure, at the nominal resolving power of $R=70,000$. Up to about $2.5 \mu\text{m}$ dark current dominates the background from the sky in-between the sky emission lines (the non-thermal sky continuum) and from the telescope. Sky emission lines cover at most a few percent of detector pixels over this wavelength regime. An estimate of the background resulting from internal optical scatter of the bright (compared to the non-thermal continuum) OH emission lines is included in Figure 1. Beyond $2.5 \mu\text{m}$ sky and telescope thermal backgrounds dominate.

To avoid loss of sensitivity it is important to keep the thermal photon background from the instrument enclosure (TR_5 Instrument Background) below the level of the dark current (TR_3 Dark Current). Figure 2 plots the thermal background from the enclosure seen by a detector pixel as a function of enclosure temperature. Thermal background photocurrent from the enclosure at temperature T and emissivity $\epsilon(\lambda)$ is given by:

$$I_{back} = (A_{pix} \Omega_{pfov})_{proj} G \int \epsilon(\lambda) \eta(\lambda) N(\lambda, T) d\lambda \quad e^{-} s^{-1} \text{ pixel}^{-1} \quad (1)$$

where $\eta(\lambda)$ is the responsive quantum efficiency

G is the photoconductive gain – the number of electrons collected per photoelectron generated (typically 1 for photovoltaic detectors like the arrays in iSHELL and 0.5 for photoconductors)

$\epsilon(\lambda)$ is emissivity

The projected area solid angle product is:

$$(A\Omega)_{proj} = \iiint \cos\theta \sin\theta dA d\theta d\phi = 2\pi A \frac{\sin^2\theta}{2} \quad (2)$$

where A_{pix} is the area of a detector pixel

Ω_{pfov} is the pixel field of view (PFOV) in sr

$\phi=2\pi$ for a conical field of view

θ is the half angle of the cone

The Planck radiation function (spectral radiance in photons) is given by:

$$N(\lambda, T) = \frac{2c}{\lambda^4} \frac{1}{[\exp(hc/\lambda kT) - 1]} \text{ photon m}^{-2} \mu\text{m}^{-1} \text{ sr}^{-1} \quad (3)$$

where c is the velocity of light ($2.998 \times 10^8 \text{ m s}^{-1}$)

h is the Planck constant ($6.626 \times 10^{-34} \text{ J s}$)

k is the Boltzmann constant ($1.381 \times 10^{-23} \text{ J K}^{-1}$)

λ is wavelength in m

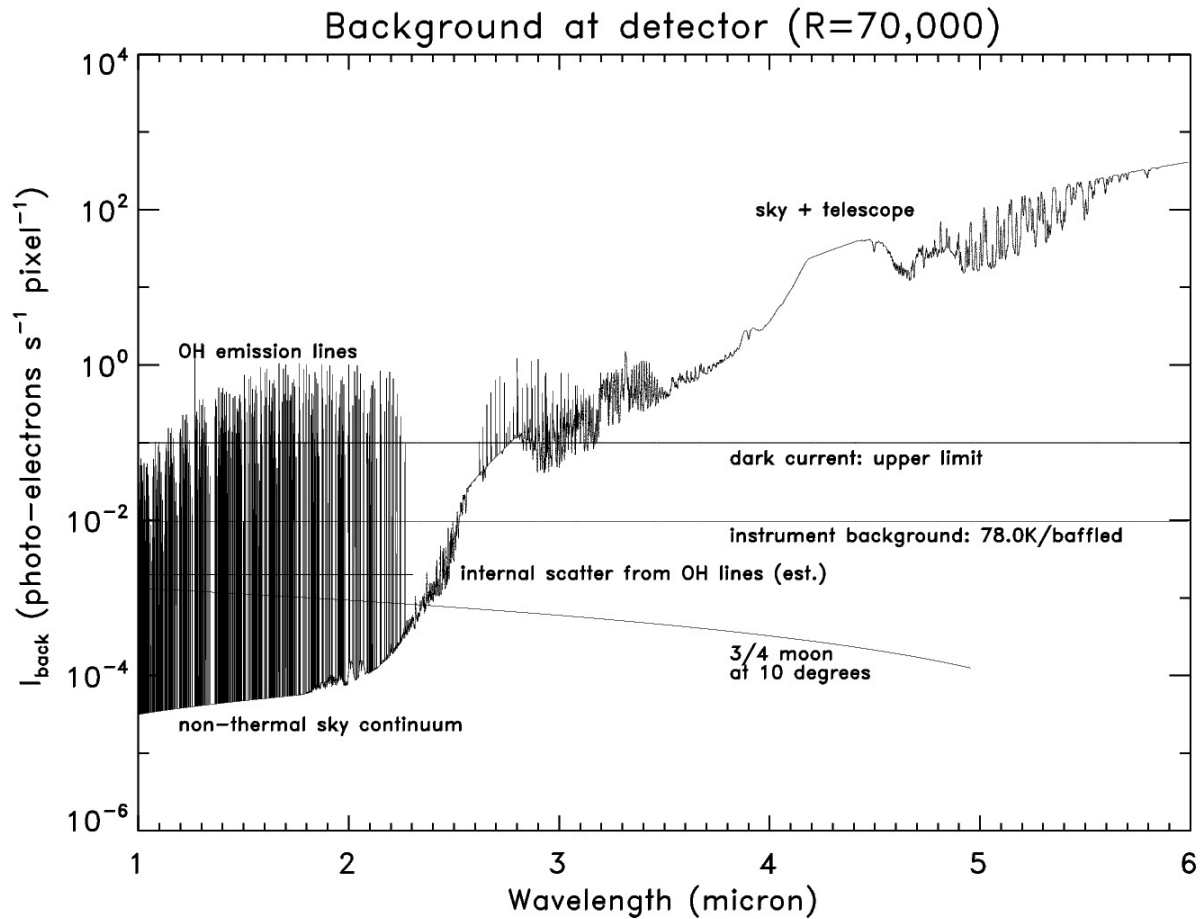


Figure 1. Background signal at a detector pixel plotted as a function of wavelength. The background sources include the telescope, sky, moon, and cooled instrument enclosure. To not limit sensitivity at short wavelengths, the background signal from the enclosure needs to be less than the detector dark current.

Inside the instrument, effectively a blackbody enclosure of temperature T and emissivity $\epsilon(\lambda) = 1$, photons from the enclosure are unfiltered and the detected signal therefore depends on quantum efficiency $\eta(\lambda)$. The Planck function is integrated across the sensitive wavelength range of the detector. For the H2RG a ‘top hat’ QE of $\eta(\lambda) \approx 0.9$ for $\lambda = 0.5 - 5.4 \mu\text{m}$ is used. The QE and the long wavelength cut-off limit of $5.4 \mu\text{m}$ ($\eta(\lambda) \rightarrow 0$) come from the H2RG data sheet provided by the vendor, Teledyne. A plot is also shown for a cut-off wavelength of $5.5 \mu\text{m}$ to assess the effect of uncertainties in the precise cut-off wavelength combined with the exponential increase of detectable photons from the enclosure with increasing wavelength. Plots are shown for a 2π steradian PFOV and for a PFOV limited by a 38 K baffle attached to the detector (half-angle 15 degrees – limited by the length of the baffle between the array mount and final camera lens).

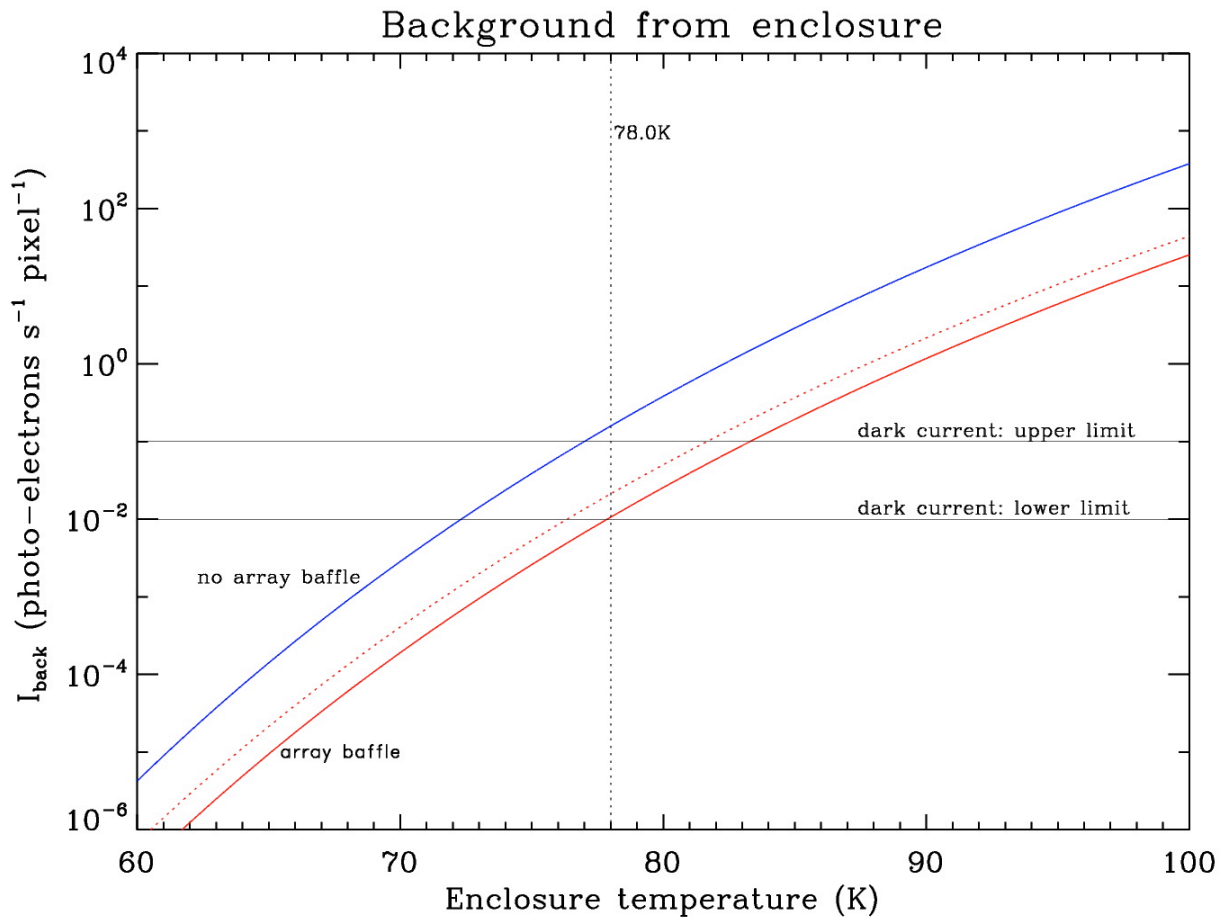


Figure 2. Background signal at a detector pixel is plotted as a function of enclosure temperature. The blue plot is for a 2π steradian FOV (90 degree half-angle), and the red plot is for a half-angle FOV of 15 degrees (the practical limit for the iSHELL optical design) where the PFOV is limited by a baffle at the same temperature as the detector array (38 K). Both plots assume a detector cut-off of $5.4 \mu\text{m}$. The dashed-red plot is the same as the red plot except for a cut-off wavelength of $5.5 \mu\text{m}$. The upper and lower limits for detector dark current are shown. Keeping the enclosure temperature below about 78 K will ensure that dark current limits sensitivity and not the cryostat when a cold baffle restricts the detector FOV. This can be achieved with a liquid nitrogen cooled enclosure (about 74 K).

The advantage of baffling the detector is that a higher temperature enclosure can be used – about 78 K compared to about 72 K for an unbaffled detector (2π sr PFOV). The former can be achieved with liquid nitrogen (boiling point 74 K at the altitude of Mauna Kea) whilst the latter requires solid nitrogen (triple point about 63 K) or more practically a closed-cycle cooler. Baffling the detector field of view also shields the detector from possible local hot spots and leaks in the enclosure (see Figure 3). The disadvantage is that optical optimization cannot move optical elements closer to the array than about 100 mm where optical performance might be improved.

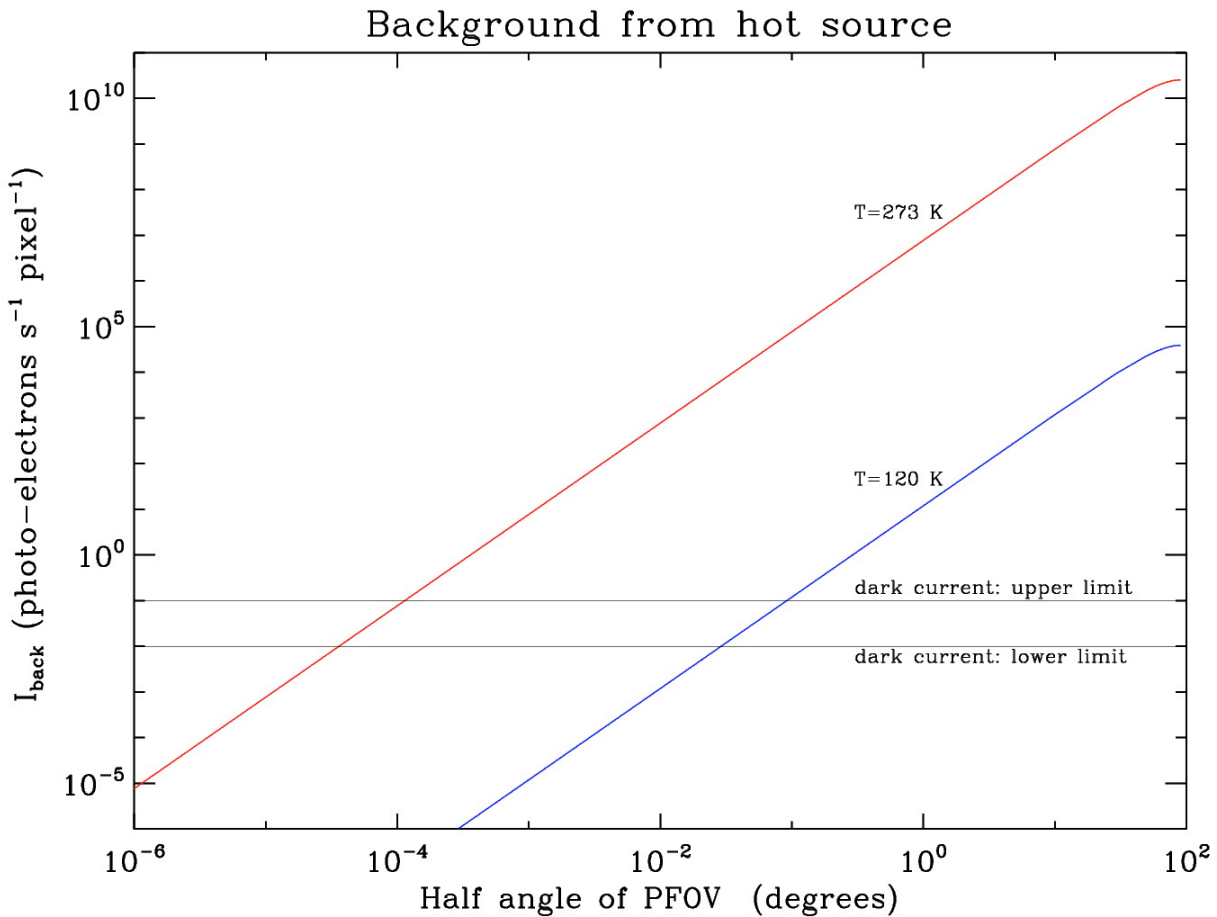


Figure 3 . Background signal from blackbody sources at 273 K and 120 K at a H2RG detector pixel is plotted as a function of the half angle of the pixel field of view. A hot source (e.g. a wire or pinhole leak in the cryostat enclosure) only needs to subtend a very small angle at a detector pixel to become a significant source of background. The detector is assumed to have a top hat QE of $\eta(\lambda)=0.9$ from $0.5\text{-}5.4 \mu\text{m}$.

Another fundamental requirement of the thermal design is to cool the detector arrays sufficiently to minimize dark current and maximize sensitivity. This means operating the H2RG array (spectrograph) and the Aladdin InSb array (slit viewer) at about 38 K and 30 K respectively. Also, to further reduce noise and for electronic bias stability, the arrays must be controlled to better than ± 0.1 K.

For long term radial velocity stability the position of spectra on the spectrograph array need to be stable to better than 0.1 pixels, a shift which will result from a temperature change of 0.1 K in the Silicon immersion gratings (due to refractive index changes). Also, the immersion gratings need to operate at a temperature above the thermal sink temperature to afford some level of thermal control but not warm enough to result in significant background emission. A good compromise is 80 K for a liquid nitrogen sink (see Section 3.3.2).

2.2 Practical requirements

In any practical cryostat parasitic heat loads need to be minimized to reduce the cooling requirements on the chosen cooling scheme (e.g. volume of liquid cryogens, capacity of a closed-cycle cooler). Minimizing the surface area and emissivity of the cooled enclosure minimizes heat radiation loads. Operating the cryostat under vacuum minimizes gas conduction loads. Where heat-conducting paths connect warm and cold components such as the mechanical support structure and wiring for array operation and instrument control, the requirements are opposite. Rigid mechanical support is achieved with short connections (L) and thick cross-sectional areas (A), i.e. by maximizing A/L , but this condition maximizes the conducted heat load. Similarly, short and thick wires are optimum for electrical performance but not for heat loads. Working solutions result from design trade-offs and choice of suitable materials.

Cooling times are also an important consideration. Cool down and warm up times of no longer than about three days, resulting in cycle times of less than one week, are very helpful, particularly during instrument testing and for operational maintenance and troubleshooting. Cool down and warm up times much shorter than about 12 hours (about 0.5 K/min) risk thermal shock to the optics (TBC). (A thermal FEA analysis of the lenses is being done). Cycle times are proportional to the cold mass of the instrument. Therefore minimizing the cold mass is good, particularly for components like filter wheels that are not usually strongly conductively connected to a cold sink and cool mostly through radiation.

There are no specifications from the array vendors Teledyne (H2RG) and Raytheon (Aladdin) on the maximum cooling and warming rates of the detector arrays. In lab tests Raytheon have not had any problems at cooling rates of about 1 K/min. Teledyne have modified the design of the H2RG arrays to fix failures related to thermal stress. Since the fix no failures related to thermal stresses have been reported, including arrays that were dunked in liquid nitrogen. The Aladdin arrays in SpeX are cooled at an average rate of 0.4 K/min and these arrays have shown no signs of thermal stress (e.g. disconnected pixels) over one decade of operation. Therefore, to be conservative, and given the desired long life of the arrays in iSHELL, we require that the cooling and warming rates of the detector arrays be < 0.5 K/min.

2.3 Summary of high-level thermal design requirements

1. Optical enclosure temperature < 78 K, stability < 1 K
2. Detector array cooling/warming rate < 0.5 K/min
3. Optical element cooling/warming rate < 0.5 K/min (the rate measured for the SpeX optical mounts, see Figure 15 Collimator Optics)
4. Spectrograph array temperature ~ 38 K, stability < 0.1 K
5. Guider array temperature ~ 30 K, stability < 0.1 K
6. Immersion grating temperature ~ 80 K, stability < 0.1 K
7. If used, liquid nitrogen hold-time must be longer than two days
8. Cooling/warming times must be no longer than three days with a goal of two days

3 CRYOSTAT CONCEPT

3.1 Design options

The optics enclosure and bench require cooling to $\leq 78\text{K}$ and the detector arrays require cooling to about 30K. A liquid nitrogen/liquid helium would work but this is not practical given the expense of liquid helium. A cryostat cooled with closed-cycle coolers would also work but given the mass and volume of the instrument at least two coolers are needed. Even then a liquid nitrogen pre-charge can or liquid nitrogen flow-through system is needed if it is required to have the instrument cool within a few days. Once cold, however, the cryostat can operate unattended. Our favored and perhaps simplest option is to use a hybrid design in which the cryostat is cooled by a combination of a closed-cycle cooler and large liquid nitrogen can. Compared to the two closed-cycle cooler option it cools the instrument faster and with less risk. However, it is not capable of unattended operation since liquid nitrogen refills are required. This approach is successfully used with SpeX.

3.2 SpeX cryostat

3.2.1 Description

The vacuum jacket consists of a four-sided center section weighing about 90 kg onto which two large O-ring sealed covers, each weighing about 35 kg, are bolted. The four-sided center section is electron-beam welded from four plates of 2219-aluminum. The external dimensions of the vacuum jacket are 112 cm x 79 cm x 61 cm. Since no hard connections are made with the vacuum jacket except at the rigid 25 mm thick top plate, stability concerns are limited to keeping the flexure well below the yield strength of the aluminum, and to keeping the flexure of shafts connecting to warm motors mounted on the vacuum jacket within the specifications of the flexible couplings. This is easily achieved using a vacuum jacket wall thickness of 12.5 mm. A spreader bar has been added between the two large covers, without which the wall thickness would have to be considerably larger. The maximum observed deflection upon evacuation is 2 mm.

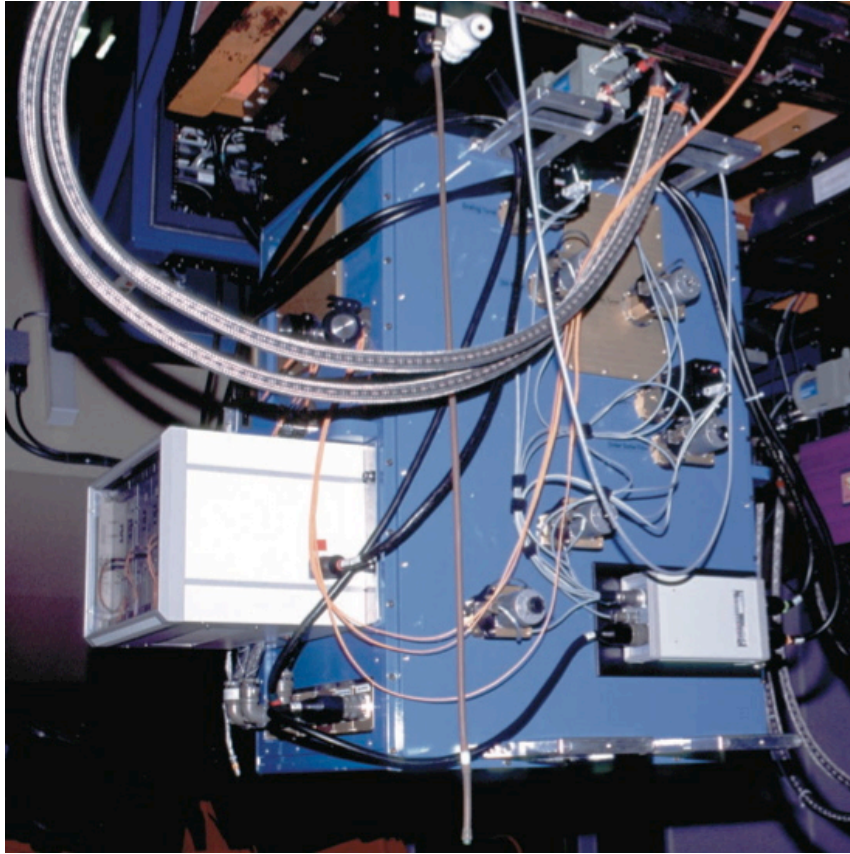


Figure 4. SpeX on IRTF. The cryostat (blue box) is mounted to the telescope by the black interface box, which contains the calibration unit. The closed-cycle cooler is visible at the top of the cryostat. Visible on the front cover of the cryostat are motors for controlling the seven cold mechanisms. Mounted to the side of the cryostat at the lower left is the cryostat-mounted electronics box containing clock, bias preamp, analog-to-digital converter, and fiber-optic boards. The MORIS CCD camera mounts to the opposite side (right). For scale, SpeX is 1.4 m tall and weighs 478 kg.

SpeX is attached to the telescope multiple instrument mount by a rigid interface box mounted to the top plate of the vacuum jacket. A spectral calibration unit is built into this box. The walls of the calibration box are 25 mm thick, and the box is 28 cm deep. The top plate of the vacuum jacket contains the entrance window, liquid nitrogen fill port, and mount for the closed-cycle cooler. The cryostat-mounted electronics box and the MORIS CCD camera box are mounted on opposite sides of the cryostat center section.

The 6061-T6-aluminum cold structure is supported on four V-shaped fiberglass support trusses that connect to the cold structure near the center of gravity. The base of the support trusses is bolted directly to the inside surface of the rigid top plate of the center section. In the interests of stiffness, the cold structure consists of a series of boxes bolted to a backbone that provides cooling and support. The total weight of the cold structure is 140 Kg. A 3 mm thick aluminum radiation shield encloses the cold structure. Four fiberglass tabs support the 30 kg radiation shield separately. The total weight of the instrument at Cassegrain focus is 478 kg.

The cooling scheme adopted in SpeX is a simple and conservative design that meets all the temperature and cooling requirements. Cooling the cold structure to liquid nitrogen temperatures is adequate to keep the instrument background below the best expected InSb detector dark current of $0.1 \text{ e}^- \text{ s}^{-1}$, since all but a half-viewing angle of 12 degrees can be shielded with a baffle at the temperature of the detector (30 K). A closed-cycle cooler is used to cool a radiation shield surrounding the cold structure, and the cold structure is attached to a LN₂ can that provides a very stable temperature. The use of a LN₂ can also speeds cooling. The surface areas of the vacuum jacket, actively cooled radiation shield, and cold structure, are 4.0 m^2 , 3.5 m^2 , and 2.0 m^2 , respectively. The actively cooled shield need only be cooled to a temperature that reduces the radiation load on the cold structure down to the level of the other parasitic loads, such as the G10 fiberglass support trusses, loads that can be accommodated by the LN₂ can. Any variation in the closed-cycle cooler performance results only in boil-off changes and not in cold structure temperature changes.

We use a two-stage 1050 CTI cryocooler to cool the radiation shield and detectors. The first stage has a rated cooling of about 70 W at 80 K, and the second stage has a rated cooling of about 8 W at 20 K. The first stage cools a highly polished 3 mm thick 6061-aluminum cold shield to less than 100 K. The resulting radiation load from the radiation shield onto the cold structure is less than 0.5 W. The estimated heat load on the cold structure consists of 2.5 W from the G10 support trusses, 2.7 W from the motor shafts, 0.4 W from the wiring, 3.0 W from the two windows, and 0.7 W from penetrations in the radiation shield. Since the heat load from the radiation shield is so small compared to the other parasitic heat loads, any normal variation in the closed cycle cooling to the radiation shield has little effect on the temperature of the enclosed cold structure. Larger temperature excursions of typically 0.5 K result from changes in the level of LN₂ as a result of boil-off, but this is too small to have any measurable impact on instrument performance (e.g. focus or instrument background). The calculated hold-time of the 10 l capacity LN₂ can compares well with the measured hold-time of about 36 hr. The bulk of the 140 kg cold structure cools to 80 K in about 24 hr at which time all the mechanisms function normally. Since there is little conduction cooling through the bearings of the filter wheels and turrets, the surfaces of these wheels are painted black to speed cooling by radiation. The instrument background measured at the spectrograph detector falls to $300 \text{ e}^- \text{ s}^{-1}$ at 24 hr, $5 \text{ e}^- \text{ s}^{-1}$ at 48~hr, and bottoms out at $\sim 0.1 \text{ e}^- \text{ s}^{-1}$ after 72 hr. About 150 l of LN₂ is required to reach the operational temperature at 48 hr.

The spectrograph and slit-viewer arrays are located close together, at the end of the cryostat opposite to the closed-cycle cooler. The array mounts are cooled via a 0.8 m-long copper strap with a cross-sectional area of about 80 mm^2 . Each of the array mounts, including cold baffle snouts, weigh about 0.9 kg and take 11 hr to cool to the operating temperature of 30 K. Using heater resistors, each mount is controlled to $30.00 \pm 0.01 \text{ K}$ by a Lakeshore model 330 temperature controller. Warm-up also takes 48 hr. To avoid precipitating ices on the detectors during warm-up, the arrays are warmed for a few hours before the cryocooler is turned off. After turning off the cryocooler and blowing out the LN₂, warm-up of the cryostat is accelerated by circulating warmed dry air through the LN₂ can.

3.2.2 Thermal analysis methods

Radiation

The net radiated heat transfer from a body at temperature T_2 and area A_2 onto a body at temperature T_1 and area A_1 is given by:

$$Q = \sigma A_1 F_e F_a (T_2^4 - T_1^4) \quad (4)$$

where Q is the heat flow (W)

σ is the Stefan-Boltzmann constant ($5.67 \times 10^{-8} \text{ Wm}^{-2}\text{K}^{-4}$)

F_e is the emissivity factor

F_a is the configuration factor

The emissivity factor accounts for the emissivities of the surfaces. The configuration factor accounts for the geometrical configuration of the surfaces. For complex geometries the configuration factor is derived by a ray-tracing (Monte Carlo) analysis. Some useful geometries for analyzing cryostats are as follows (e.g. The Infrared Handbook, editors Wolfe & Zissis 1978):

For concentric spheres or infinite cylinders, $F_a=1.0$ and

$$F_e = \frac{1}{\left[1/\varepsilon_1 + \frac{A_1}{A_2}(1/\varepsilon_2 - 1) \right]} \quad (5)$$

For infinite parallel planes, $F_a=1.0$ and

$$F_e = \frac{1}{(1/\varepsilon_1 + 1/\varepsilon_2 - 1)} \quad (6)$$

For parallel rectangles (see Figure 5), $F_e = \varepsilon_1 \varepsilon_2$ and F_a is estimated from the view factors plotted in Figure 6 (a).

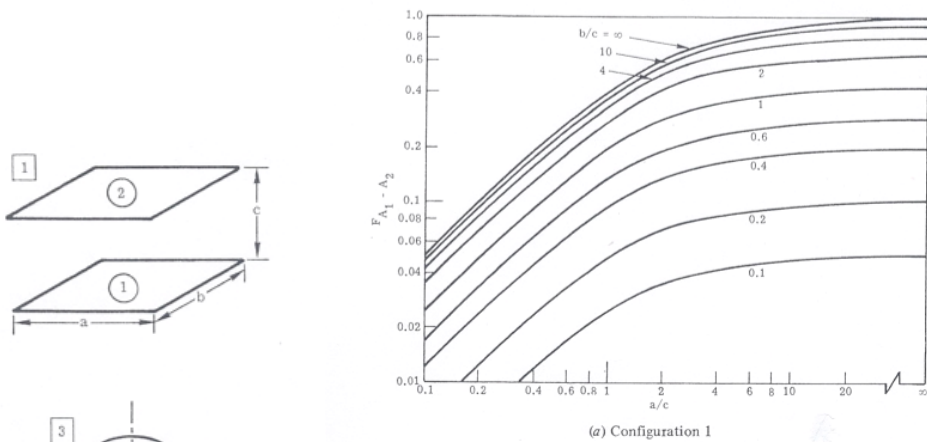


Figure 5. Parallel rectangles (1) and parallel disks (2)

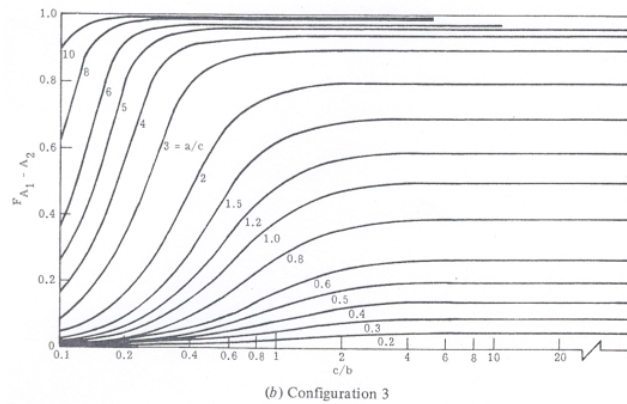


Figure 6. Configuration factors for parallel rectangles (a) and parallel disks (b)

For parallel disks (see Figure 5), $F_e = \epsilon_1 \epsilon_2$ and F_a is estimated from the view factors plotted in Figure 6 (b).

Conduction in solids

Fourier's Law gives the fundamental equation for one-dimensional heat transfer:

$$Q = kA \frac{dT}{dx} \quad (7)$$

where Q is the heat flow (W)

k is the thermal conductivity of the material ($Wm^{-1}K^{-1}$)

A is the cross-sectional area through which the heat flows normal to the direction of heat flow

dT/dx is the temperature gradient at the section in the direction x of the heat flow

In this formulation edge effects are assumed to be negligible. To a very good approximation, most conduction problems encountered in cryogenic design can be considered to be one-

dimensional. For most materials the thermal conductivity varies considerably with temperature. For a thermal conductor of length L and cross-sectional area A , Equation 7 can be rewritten in the form:

$$Q = \frac{A}{L} \int_{T_1}^{T_2} k dT = \frac{A}{L} \left(\int_{T_{ref}}^{T_2} k dT - \int_{T_{ref}}^{T_1} k dT \right) \quad (8)$$

The integral of k with respect to temperature is known as the Thermal Conductivity Integral and is tabulated for a number of materials (units Wm^{-1}).

For structures penetrating into the cold optical enclosure, in addition to heat flowing through the conductor, heat is also radiated away from its surface. Radiation losses are most significant for thermal isolators such as support legs and drive shafts that effectively act like radiators inside the cryostat and can sometimes dominate the conducted heat loads from these structures. The radiated heat loads can be estimated by piecewise integration of the temperature gradient along the structure. In SpeX this is done for the fiberglass supports, fiberglass drive shafts, and PVC ribbon cabling.

The temperature drop across a thermal conductor due to heat flowing through it is analogous to the voltage drop across an electrical conductor (or resistor) due to the flow of an electrical current. Using Equation 7, we can define a thermal resistance R by:

$$R = \frac{\Delta T}{Q} = \frac{1}{k} \frac{\Delta x}{A} \quad (9)$$

In a thermal circuit it is easy to show that for as one-dimensional heat flow, the total thermal resistance R_T , of n thermal conductors connected in series is simply:

$$R_T = R_1 + R_2 + \dots + R_n = \sum_{i=1}^n \frac{1}{k_i} \frac{\Delta x_n}{A_n} \quad (10)$$

This formulation is used when estimating heat flows and temperature drops of conductors in series, for example when connecting the detector to the second stage of the closed-cycle cooler.

By analogy, for thermal resistances in parallel:

$$\frac{1}{R_T} = \frac{1}{R_1} + \frac{1}{R_2} + \dots + \frac{1}{R_n} \quad (11)$$

In practice, when thermal resistances are connected together, an additional temperature drop will occur due to imperfect contact at the interface. By definition, the thermal contact resistance is given by:

$$R_m = \frac{\Delta T_{in}}{A_{in} q_{in}} = \frac{1}{A_{in} h_{in}} \quad (12)$$

where q_{in} is the heat flowing through the interface per unit area

A_{in} is the apparent contact area of the interface

ΔT_{in} is the temperature drop across the interface

h_{in} is defined as the thermal interface conductance

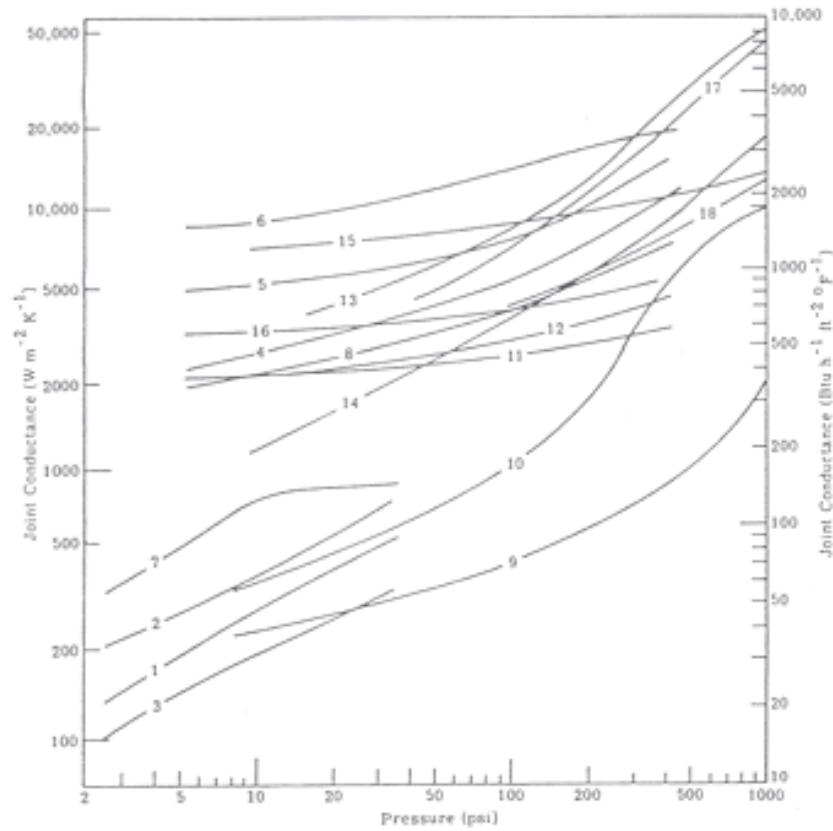
Heat transfer through the interface takes place by the combined mechanism of conductance across true contact areas, conduction across entrapped interstitial fluids, and radiation across interstitial gaps. The resulting overall conductance of the interface is a function of the material in contact (conductivity, surface finish, flatness, and hardness), the contact pressure, the mean temperature of the interface, the nature of the interstitial fluid (liquid, gas, vacuum), and the presence of oxide films or interstitial shim materials. The apparent contact area A_{in} is just the surface area of the interface (which is not necessarily in contact). The actual material-to-material contact area A_c is contained within the definition of the interface conductance and so $h_{in} \propto A_c$. From simple elastic deformation theory it follows that:

$$h_{in} \propto \frac{1}{E} \frac{F}{A_{in}} \quad (13)$$

where E is Young's modulus (Nm^{-2})

F/A_{in} is the tensile stress or pressure due to the tensile force F

Figure 7 is a plot of the thermal interface conductance against contact pressure for a variety of materials and conditions. As predicted, the conductance increases with pressure. Significant increase in interface conductance can be obtained by the application of interstitial fluids such as silicone high vacuum grease (a factor of five on brass surfaces, see Clausing and Chao. 1965, *Journal of Heat Transfer*, 27, 243), and interface shim materials which are softer than the interface. These improvements are due to an effective increase in the area of contact.



Curve	Material Pair	rms Surface Finish (µin.)	Gap Material	Mean Contact Temp. (°F)
1	Aluminum (2024-T3)	48-65	Vacuum (10 ⁻⁴ mm Hg)	110
2	Aluminum (2024-T3)	8-18	Vacuum (10 ⁻⁴ mm Hg)	110
3	Aluminum (2024-T3)	6-8 (not flat)	Vacuum (10 ⁻⁴ mm Hg)	110
4	Aluminum (75S-T6)	120	Air	200
5	Aluminum (75S-T6)	65	Air	200
6	Aluminum (75S-T6)	10	Air	200
7	Aluminum (2024-T3)	6-8 (not flat)	Lead foil (0.008 in.)	110
8	Aluminum (75S-T6)	120	Brass foil (0.001 in.)	200
9	Stainless (304)	42-60	Vacuum (10 ⁻⁴ mm Hg)	85
10	Stainless (304)	10-15	Vacuum (10 ⁻⁴ mm Hg)	85
11	Stainless (416)	100	Air	200
12	Stainless (416)	100	Brass foil (0.001 in.)	200
13	Magnesium (AZ-31B)	50-60 (oxidized)	Vacuum (10 ⁻⁴ mm Hg)	85
14	Magnesium (AZ-31B)	8-16 (oxidized)	Vacuum (10 ⁻⁴ mm Hg)	85
15	Copper (OFHC)	7-9	Vacuum (10 ⁻⁴ mm Hg)	115
16	Stainless/aluminum	30/65	Air	200
17	Iron/aluminum	-	Air	80
18	Tungsten/graphite	-	Air	270

Figure 7. Thermal contact conductance versus pressure (from Wolfe and Zissis 1978). Examples of measured contact conductance data h_i as a function of contact pressure are given in the accompanying table for the interface conditions listed.

Conduction in gases

The when the mean free path is greater than the dimensions of the apparatus the conducted heat flow between concentric spheres, coaxial cylinders, or parallel planes is given by (Corruccini, R.J., 1959, *Vacuum*, 7-8, 19):

$$\frac{H}{A_1} = a \frac{\gamma + 1}{\gamma - 1} \left(\frac{R}{8\pi} \right)^{\frac{1}{2}} \frac{P}{(MT)^{\frac{1}{2}}} (T_2 - T_1) \quad (14)$$

$$a = \frac{a_1 a_2}{a_2 + a_1 (1 - a_2) A_1 / A_2}$$

where a is the overall accommodation coefficient and A_1 / A_2 is the geometrical configuration factor

H is the net heat flow per unit time

γ is C_p / C_v , the specific heat ratio of the gas, assumed constant

a_1 is the accommodation coefficient of the inner surface

a_2 is the accommodation coefficient of the outer surface

R is the molar gas constant

P the gas pressure

M is the molecular weight of the gas

T is the effective gas temperature

A_1 is the area of the inner surface, temperature T_1

A_2 is the area of the outer surface, temperature T_2

The constant $(R/8\pi)^{1/2}$ has the value 0.2426 for H in W cm^{-2} , P in mm Hg, and T in K.

Writing Equation 14 explicitly for nitrogen gas (air) , assuming $a_1 = a_2 = 0.5$ (reasonable for surfaces typically encountered in cryostats), and a geometry corresponding to co-axial cylinders ($A = A_1 = A_2$), we obtain:

$$\frac{H}{A} = BP(T_2 - T_1) \quad (15)$$

Where H/A is the heat flow in Wm^{-2}

B is $30 \text{ Wm}^{-2}\text{K}^{-1}\text{mbar}^{-1}$ for N_2 and $5.3 \text{ Wm}^{-2}\text{K}^{-1}\text{mbar}^{-1}$ for H_e

P is the gas pressure in mbar measured at the room temperature gauge

At the pressures of $< 10^{-5}$ routinely obtained in cryostats the heat load due to gas conduction from room temperature to about 75 K is $\sim 0.01 \text{ Wm}^{-2}$, insignificant compared to other heat loads.

Cooling

Liquid nitrogen provides at heat sink temperature of about 74 K at the altitude of Mauna Kea (0.6 atm.). It is useful to express a cryogens cooling ability in terms of its density (ρ) and latent heat of vaporization (L_v) product. In the appropriate units:

$$(\rho L_v)_{LN_2} = 44.7 \text{ W hr l}^{-1} \quad (16)$$

This would mean that a 10 W heat load would boil away 10 liters of LN₂ in 44.7 hours.

Closed-cycle coolers do not provide a constant temperature heat sink since cooling efficiency depends on the applied heat load. The typical refrigeration capacity of a CTI-CRYODYNE 1050 CP cryocooler of the type used in SpeX is shown in Figure 8.

Model 1050 Cryodyne Refrigeration System



The Model 1050 is available in both single and two stage configurations to meet a variety of high capacity cooling applications. The M-1050 is ideal for a number of High Temperature Superconductor applications that require cooling from 20K to 80K.

The M-1050 single stage system will provide 80 watts of heat lift at 77K. The M-1050 two stage system will provide 7 watts of heat lift at 20K and 65 watts at 77K simultaneously.

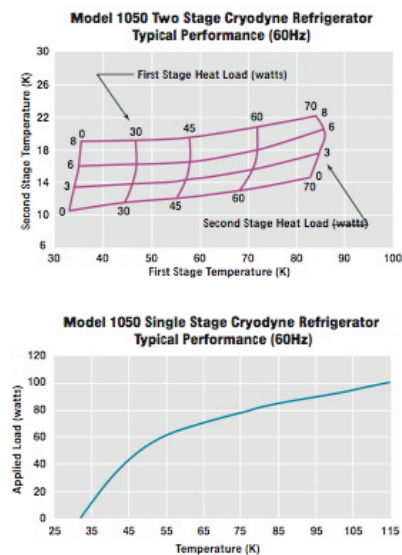


Figure 8. Cooling capacity of CTI-CRYODYNE 1050 CP cryocooler

The cooling time for a mass connected to a temperature sink is simply the enthalpy of the mass divided by the cooling rate. More rigorously for a mass that cools by conduction through a conductor connected to a heat sink and by radiation to an enclosure at the temperature of the heat sink (e.g. a filter wheel), the incremental cooling time is given by:

$$\text{Cooling time } (T_i \text{ to } T_{i+1}) = \frac{mc_p(T_i)[T_i - T_{i+1}]}{(A/L)k(T_i)[T_i - T_{sk}] + \sigma A_s F_e F_a [T_i^4 - T_{sk}^4] - Q(T_i)} \quad \text{where } T_i > T_{i+1} \quad (17)$$

where T_i is the initial temperature

m is the mass of specific heat c_p to be cooled

T_{sk} is the temperature of the sink (e.g. 74 K for LN₂)

A is the cross-sectional area of the connecting conductor, length L , thermal conductivity k

A_s is the surface area of the radiator, emissivity factor F_e , configuration factor F_a

$Q(T_i)$ is the heat input to the mass at temperature T_i

For small cooling intervals $k(T_i) \approx k(T_{i+1})$ and $c_p(T_i) \approx c_p(T_{i+1})$. The total cooling time is then just the summation of Equation 17 over the individual cooling intervals. The equation is not valid for systems in which the mass of the conductor is similar to the mass to be cooled. For example, when a liquid nitrogen can is attached directly to an optical bench. Under those circumstances the cooling time is largely dependent upon how efficiently the cooling liquid can be kept in contact with the can as it vaporizes.

3.2.3 Cryostat thermal model

SpeX uses a 10 liter capacity liquid nitrogen can to cool the optical bench and enclosure. To reduce the radiated heat load from the warm vacuum jacket onto the cold optical enclosure the optical enclosure is surrounded by a polished aluminum cold shield that is actively cooled by connecting it to the first stage of a 1050 CP cryocooler. The other parasitic heat loads include the support structure, drive shafts, wiring, and cryostat windows. The calculated heat loads are approximate since the emissivities and viewing geometries are not precisely known.

Active shield

The active shield is designed to reduce the radiated heat load onto the liquid-nitrogen cooled optical enclosure to less than about 10% of the other parasitic heat loads onto the optical enclosure (~10 W). This requires the active shield to be cooled to an average temperature of less than about 110K. With cooling provided by the cryocooler the active shield must be thick enough for an acceptable temperature gradient along the length of the shield but not too thick to add unnecessarily to the mass. Also the thermal resistance of the connection between the cooler and the shield needs to be minimized by increasing A/L but not enough to

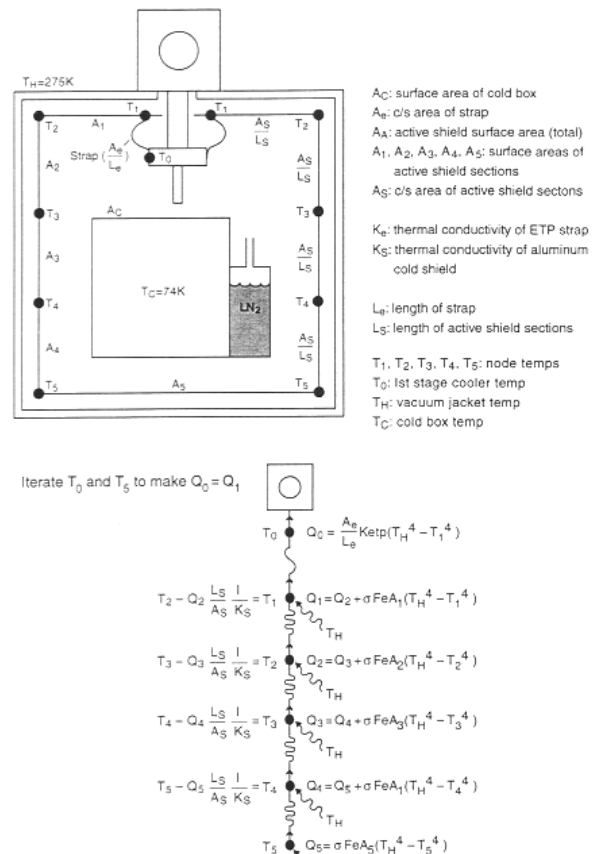


Figure 9. Spex active thermal shield model

make it too inflexible. Figure 9 shows the simple thermal network that was used to find a solution.

With a 3mm thick aluminum shield (30 kg) and an OFHC copper foil strap ($A/L=0.39$ m) an average active shield temperature of about 100 K is achieved. The operating temperature of the cryocooler first stage is about 52 K, indicating a heat load of 35 W (see Figure 8). From Equations 4 and 5 this implies an aluminum shield emissivity of $\epsilon_1 = \epsilon_2 = 0.07$, which is in agreement with expectations for highly polished aluminum. The radiated heat load onto the cold structure (surface area 2 m^2) is about 0.4 W, assuming a concentric spheres approximation with $F_a=1.0$ and $F_e=0.05$ (see Equations 4 and 5).



Figure 10. The cryostat showing the vacuum jacket, cryocooler, active radiation shield (partial), liquid nitrogen can mounted to the spectrograph box, and support trusses. The fore-optics box is not installed.

Support truss

Four V-shaped fiberglass trusses support the 140 kg cold structure. Individual truss legs are 313 mm long with a free length of 223 mm and a cross-sectional area of 645 mm^2 (50.8 mm x 12.7 mm) for a total $A/L=0.023$ m. The conducted heat load is 2.5 W. The radiated heat load is 0.1 W, assuming a parallel plane geometry (see Figures 5 and 6) with $F_a=1.0$ and $F_e=0.7$, and a linear temperature gradient.

Motor drive shafts

Seven fiberglass drive shafts connect the cold mechanisms to externally mounted warm motors. These shaft have an average free length of 190 mm and a cross-sectional area of 44 mm^2 (arrow-flight tube with a 7mm diameter and a 1 mm wall thickness) for a total $A/L=1.6 \times 10^{-3} \text{ m}$. The conducted heat load is 0.2 W. The radiated heat load is 2.5 W, assuming an infinite parallel cylinder geometry (see Equations 4 and 5, $A_1 \ll A_2$) with $F_a=0.6$ and $F_e=0.05$, and a linear temperature gradient.

Wiring

The array wiring consists of six 50 mm wide and 1 mm thick PVC ribbon cables each about 300 mm long and each containing 32 AWG 30 manganin wires (similar to constantan). The conducted heat load from the wires ($A/L=3.2 \times 10^{-5} \text{ m}$) is about 0.1 W and from the PVC ribbons ($A/L=1.0 \times 10^{-3} \text{ m}$) about 0.1 W. The configuration geometry is difficult assess (see Figure 11) but assuming the ribbon cables run parallel to the spectrograph box the geometry is plane parallel (see Figures 5 and 6) with $F_a=0.7$ and $F_e=0.05$, and the radiated heat load is $\sim 0.1 \text{ W}$.

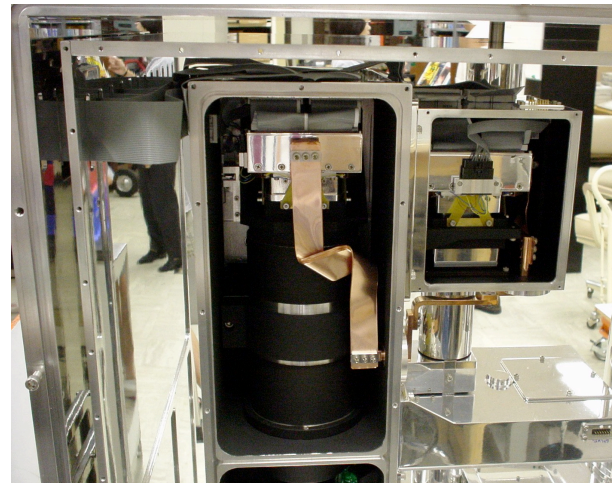


Figure 11. Array ribbon cables entering the cryostat (left) and connecting to the two arrays. Also shown is some of the thermal strapping for detector temperature control.

PVC ribbon cabling also carries instrumentation wiring but since the cables are much longer the conducted heat load is insignificant. Since the surface area is similar to the array wiring the radiated heat load is similar ($\sim 0.1 \text{ W}$).

Cryostat windows

The cryostat has square entrance and exit windows (optical port), both about 75 mm x 75 mm in size. The geometry is plane parallel (see Figures 5 and 6) with $F_a=1.0$ and $F_e=0.5$ ($\epsilon_1 = \epsilon_2 \sim 0.8$), and the total radiated heat load is $\sim 3.0 \text{ W}$.

Support bar

A highly polished aluminum spreader bar has been added between the two large covers, without which the wall thickness would have to be considerably larger. The bar is 0.61 m long with a diameter of 25 mm and penetrates into the cooled enclosure. The geometry is approximated by two infinite cylinders ($A_1/A_2 \sim 0$) with $F_a=1.0$ and $F_e=0.07$ ($\epsilon_1 = 0.07$), and the total radiated heat load is about 1.1 W.

Holes in active radiation shield

The active shield has about 30 penetrations for the support (8), motor drive shafts (7), support bar (2), LN₂ can (1), cryocooler (1), wiring (~ 10), for a total estimated area of $2 \times 10^{-2} \text{ m}^2$ (14 cm x 14 cm). Assuming a plane parallel geometry with $F_a=1.0$ and $F_e=0.1$ ($\epsilon_1=0.1$, $\epsilon_2 \sim 1.0$), the radiated heat load is 0.7 W.

LN₂ can neck tubes

The warm part of the fiberglass neck tubes does not penetrate into the cooled enclosure and the evaporating cold N₂ gas removes most of the conducted heat load. Consequently the heat load is about zero.

Estimated static heat load

The estimated total static heat load is 10.8 W (see Table 1).

Table 1. Estimated static heat load on LN₂ sink

Source	Heat load/W
Active shield	0.4
Holes in active radiation shield	0.7
Support bar	1.1
Windows (2)	3.0
Fiberglass support truss	2.5
Fiberglass motor drive shafts (7)	2.7
Fiberglass neck tubes	0.0
Wiring	0.4
Gas conduction	<0.01
Total	10.8

Detector cooling and temperature control

A schematic of the cooling scheme for the detector arrays is shown in Figure 12 and a mechanical drawing of the arrangement is shown in Figure 13. The detector mounts are connected to the second stage of the cryocooler by a series of copper (ETP) rods and (OFHC) foils (see also Figure 11). Flexible foils are required at the spectrograph detector end of the connection to accommodate a focus movement of several mm, and at the cryocooler end for ease of maintenance (occasional cryocooler replacement).

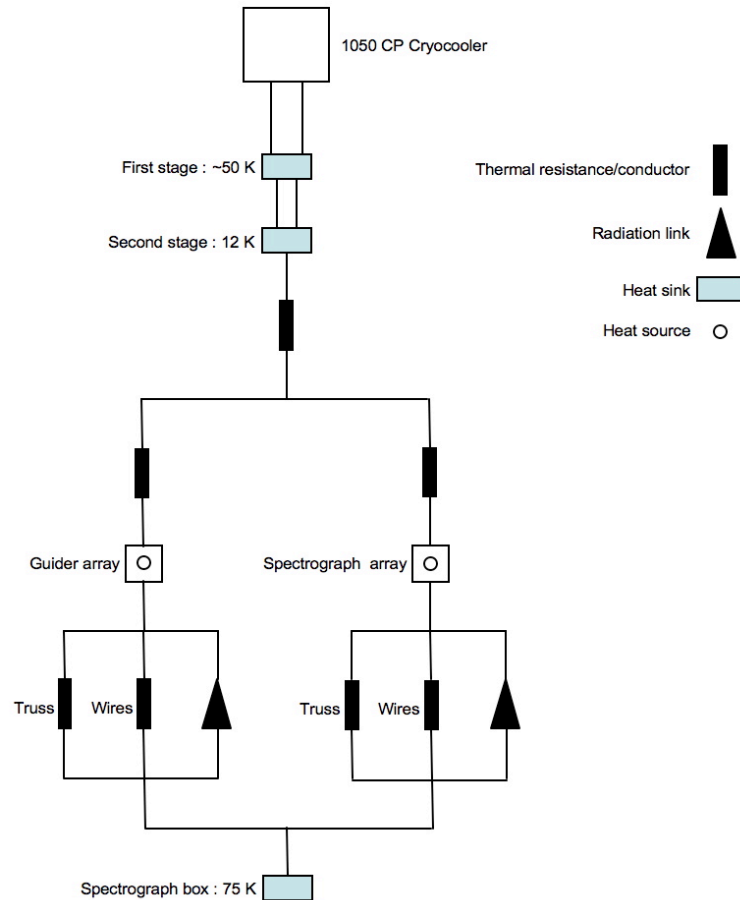


Figure 12. Detector cooling thermal circuit

Fiberglass trusses ($A/L=5.3 \times 10^{-3}$ m for eight V-shaped trusses, four per mount) rigidly mount the detector housings (each about 1 Kg) to the aluminum fixtures in the spectrograph and guider boxes (see Figure 14). Cooling is via conduction to the second stage ($A/L=0.75 \times 10^{-4}$ m) and by radiation ($F_a=1.0$ and $F_e=0.065$, $A_1/A_2 \sim 1$, $A_1 \sim 0.1$ m² for each polished aluminum detector housing). The estimated cooling time of about 14 hours to 50 K compares well to the measured time of 11 hours (about 0.4 K/min).

The static (parasitic) heat load into the spectrograph array mount comes from the fiberglass trusses (45 mW), array manganin wiring (70 mW, $A/L=9 \times 10^{-5}$ m) carried by PVC ribbon cabling (15 mW, $A/L=1.5 \times 10^{-3}$ m), and thermal radiation (15 mW), for a total of about 145 mW. Similarly for the guider array mount but which has half as many manganin wires (35 mW), for a total of 110 mW. Without any further heat load the arrays would stabilize at about 16 K with the cold head at 12 K. To maintain a temperature of 30 K requires a temperature differential across the copper strap of about 18 K and a corresponding heat load of about 1.6 W (0.8 W at each detector). Resistor heaters mounted to the detector housings (see Figure 14) provide this additional heat load (100 Ω equivalent for each mount).

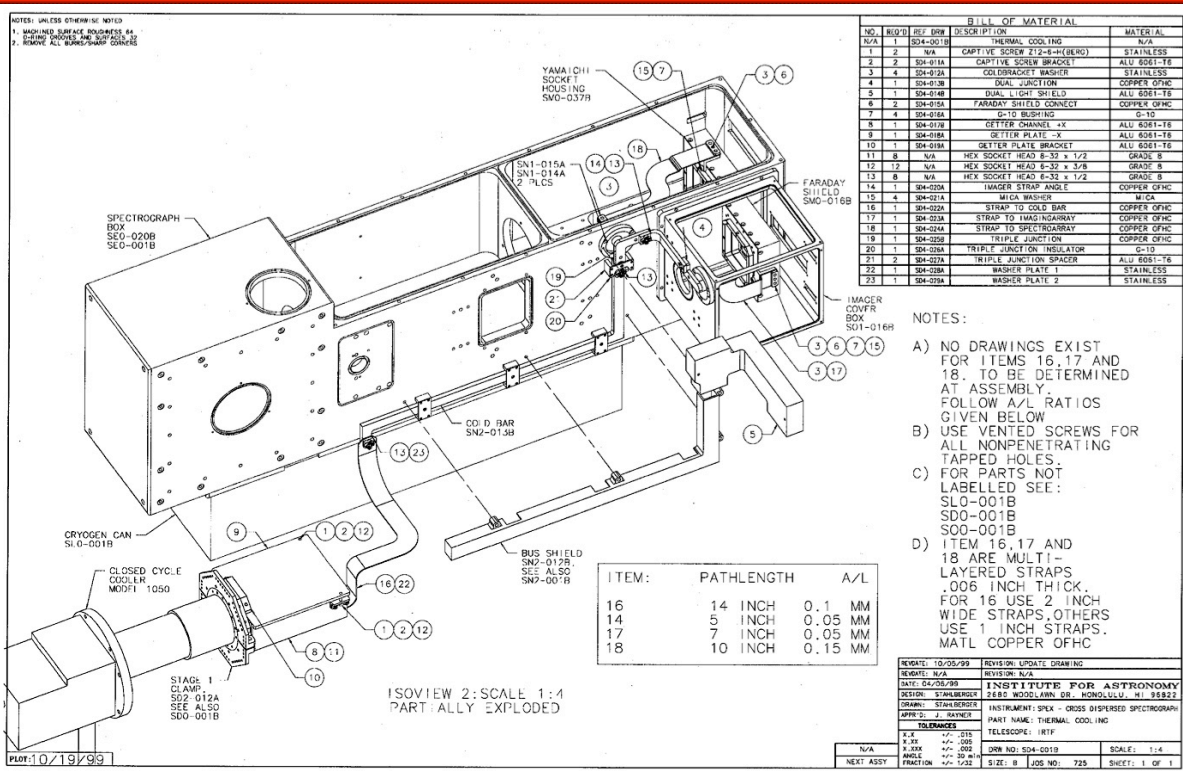


Figure 13. Detector thermal straps

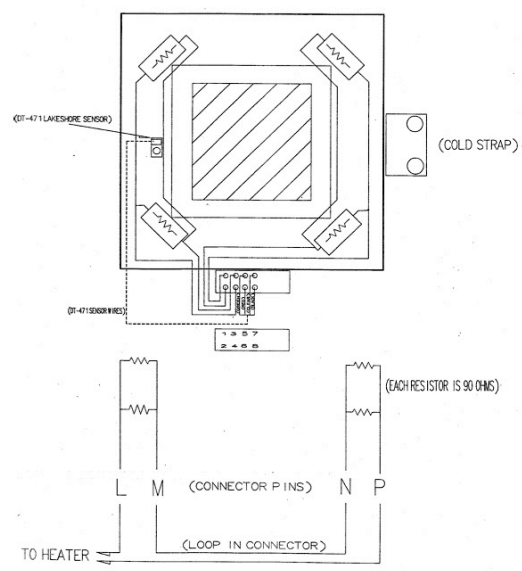
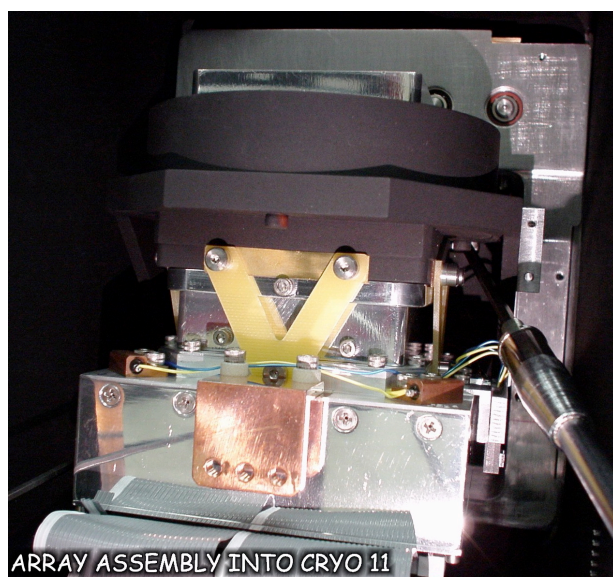


Figure 14. (Right) Spectrograph detector array mount (reflective aluminum block, 30 K) showing two of the four corner-mounted resistor heaters, the cold strap mounting point (copper), v-shaped fiberglass trusses, and spectrograph mounting structure (black, 75 K). (Left) Location of the heater resistors on the array mount, and heater circuit.

The thermal time constant of the detector array mount is estimated as follows. Since radiative cooling is negligible at the operating temperature of the arrays, the cooling rate is given by:

$$c_p m \frac{dT}{dt} = -k A/L (T(t) - T_f) \quad (18)$$

where $T(t)$, T_f are the temperature at time t and the final temperature
 c_p , m are the specific heat capacity at constant pressure, and the mass of the detector mount
 k , A/L are the thermal conductivity, and the dimensions of the conduction path

Substituting $\Delta T = T - T_f$, and $\tau = \frac{c_p m}{k A/L}$ (19)

$$\frac{d\Delta T}{dt} + \frac{\Delta T}{\tau} = 0 \quad (16)$$

This equation has the solution $\Delta T = \Delta T_0 e^{-t/\tau}$ (20)

where τ is the thermal time constant
 and ΔT_0 is the initial temperature difference ($\Delta T_0 = 30 - 18$ K for array at 30 K, cooling to $T_f = 18$ K with temperature control turned off)

From Equation 19 the calculated time constant of the detector array mount is 14 minutes (at 30 K $c_p = 35 \text{ J kg}^{-1} \text{ K}^{-1}$, $m = 2 \text{ kg}$, $k = 1.1 \times 10^3 \text{ W m}^{-1} \text{ K}^{-1}$, $A/L = 0.75 \times 10^{-4} \text{ m}$).

3.2.4 Cryostat performance

With 10 l of LN₂ the cooling capacity is 447 W hr and a static heat load of 10.8 W (see Table 1) the predicted hold time is roughly 41 hours. This compares very well with the measured hold time of about 40 hours (measured with the telescope parked at zenith during the Christmas 2010 two-day stand down).

The liquid nitrogen can is attached directly to the spectrograph and fore-optics boxes. Therefore cooling time of the bulk of the cold mass is dependent upon how efficiently the cooling liquid can be kept in contact with the can as it vaporizes, and how fast liquid nitrogen can pored into the can during cooling. (This requires two tubes – one for fill and one for exhaust.) Objects not strongly conductively coupled to the cold structure, such as mechanism wheels (bearings) and lenses (three point contact mounts), cool by a combination of conduction and thermal radiation. For optimum cooling this means making the surfaces of the mechanism wheels highly emissive. For the materials used in SpeX the lenses are opaque (highly emissive) at the wavelengths where the Planck function peaks for the lower temperatures of the optical elements inside the cryostat, which is advantageous for radiative cooling of optical materials.

Figure 15 shows the temperature at a various locations in the cryostat as a function of elapsed time for cool down (top plot) and warm up (bottom plot). The bulk of the 140 kg cold mass reaches 100 K in about five hours. The detectors cool to the operating temperature of 30 K in about 11 hours, almost lineary at an average coolong rate of about 0.45 K/min. SpeX becomes cold enough to sensitively operate once the instrument background falls below about 1 e/s at 46 hours (see Figure 16). The instrument background is too small to measure after three days (intrinsic dark current about 0.2 e/s). Since the spectrograph box cools below 80 K within about 12 hours the measured instrument background is an indicator of the temperature of the optical components in the beam (blanked off at the order sorter filter wheel) that are not conductively well coupled to the aluminum cold structure and require longer to cool. Cooling requires about 150 l of liquid nitrogen (1 liter per kg of cold mass). Once cold the average temperature of the spectrograph is 75 K. This temperature varies by about 0.5 K as the level of liquid nitrogen changes between cold fills.

If temperature control is not activated, the detectors bottom out at a temperature of about 18 K (T_f). We estimate that this requires a heat flow of about 0.4 W across the cold strap ($\Delta T = 6$ K). About 0.3 W can be formally accounted for (parasitic heat loads from the fiberglass support trusses, wiring, and thermal radiation onto the detector housings), reasonable agreement given the uncertainty in the parameters involved. Lakeshore Model 330 Temperature Controllers achieve detector stabilities of ± 0.01 K. The delivered heat load is roughly 0.5-1.0 W per mount (~ 0.1 A through 100 Ω , about 20-30% medium heater range on the controllers), consistent with the heat load required to maintain a temperature of 30 K at the warm end of the cold strap.

From Figure 15 the measured detector cooling rate is about 0.45 K/min at 30 K and the detector array mounts take about 10 minutes to cool from 30 K to 25.6 K (4.4 K = e^{-1} [30-18] K) in good agreement with the calculated time constant of 14 minutes. This means that the detector mount takes about one second to respond to temperature changes of 0.01 K, the measured stability.

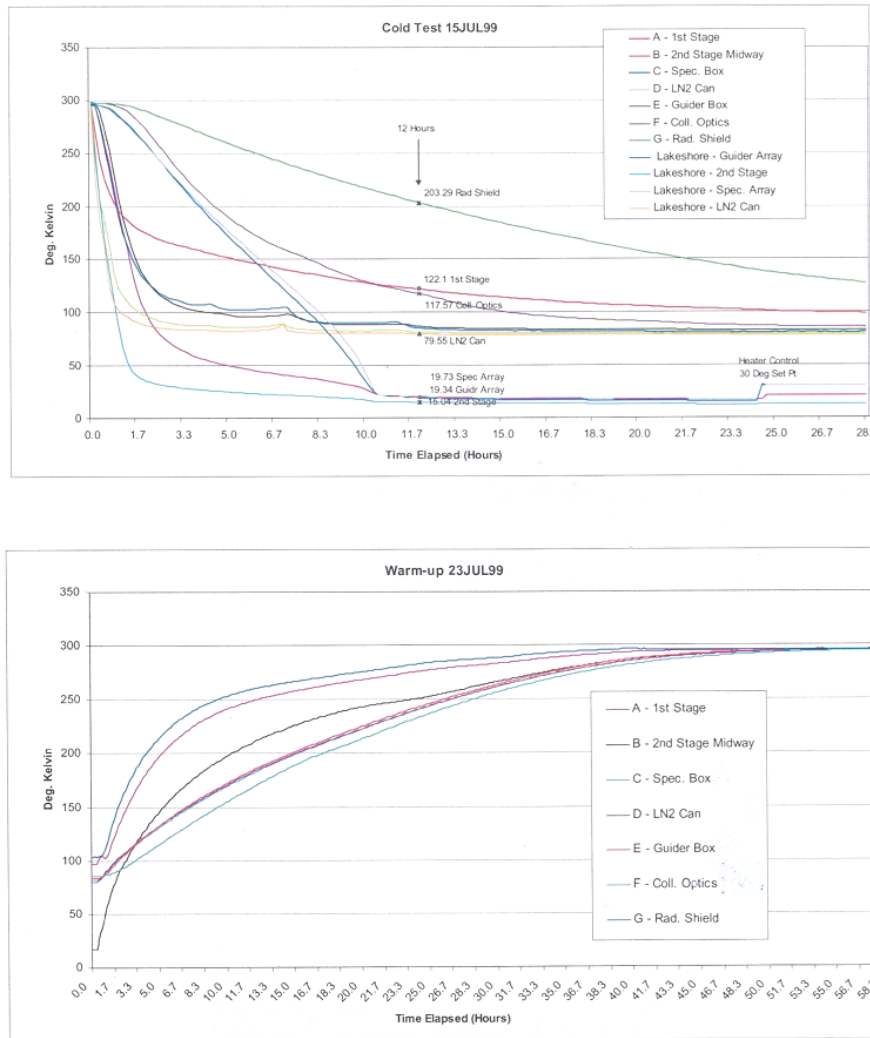


Figure 15. Cooling (top) and warming (bottom) times for SpeX.

Once liquid nitrogen is blown out and the cryocooler is turned off it takes about three days for the cryostat to reach room temperature. This can be decreased to two days by purging dry air through the liquid nitrogen can (see Figure 15).

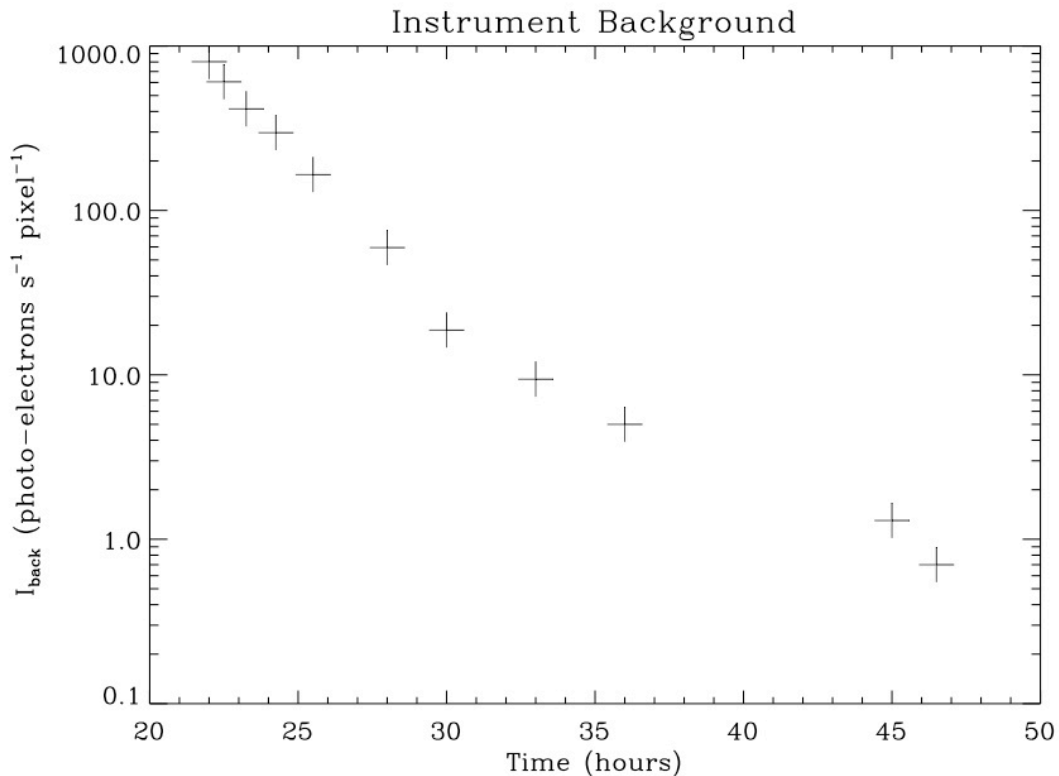


Figure 16. SpeX instrument background measurements in hours from start of cool down. SpeX becomes cold enough to sensitively operate once the instrument background falls below about 1 e/s at 46 hours. After three days the background bottoms out at 0.2 e/s - the level of the detector dark current (measured blanked-off at the detector 30 K).

3.3 Proposed iSHELL concept

3.3.1 Thermal design options

A hybrid cryostat of the type used for SpeX using a combination of a cryocooler and liquid nitrogen satisfies all the thermal requirements. An option would be to replace liquid nitrogen cooling of the cold optics with a second cryocooler. This has the advantage of providing more margin in the instrument background performance since the cryocooler can maintain temperatures of ~ 65 K, and permitting unattended operation of iSHELL if the instrument can be left in the beam. The disadvantage of this scheme is that some form of pre-cooling is required to meet the cool down time requirement, and more temperature control of the optical bench is required since its temperature is affected by the cryocooler performance. Also, the optical design would have to be re-optimized for about 70 K. For these reasons we prefer the hybrid cryostat scheme.

3.3.2 Proposed thermal design

The cryostat is of similar size to SpeX ($\approx 1\text{m}^3$) and uses the same cooling scheme. It contains an optical bench to which the optical sub-assemblies are mounted. The optics and bench are cooled to about 75K using liquid nitrogen. A tank capacity of about 10 liters is required. The radiation load on the cold structure is minimized by surrounding it with a radiation shield, which is cooled using the first stage of a Cryodyne 1050 CP closed-cycle cooler. The spectrograph and slit viewer arrays are cooled to 38K and 30K respectively, using the second stage of the cryocooler. Cooling to operational temperature will take about three days (components in the mechanism wheels take longest to cool).

There are several differences from the SpeX cryostat. The two arrays are located in separate parts of the cryostat, and each is placed close to the cryostat wall to minimize analog signal lengths for low noise performance. This requires two thermal paths to the second stage of the cryocooler instead of one. Also, cold motors will be used, removing the need for motor driveshaft feed-throughs. Precision temperature control of the immersion gratings ($\sim 80 \pm 0.1$ K) will be needed to stabilize the position of spectra to within 0.1 pixels on the spectrograph array. A longer liquid nitrogen hold time is also desirable.

The warm to 80 K cabling is almost exactly the same as SpeX, six 50 mm wide and 1 mm thick PVC ribbon cables each about 300 mm long and each containing 32 AWG 30 manganin wires (similar to constantan).

A significant difference between SpeX and iSHELL is the proposed use of cold motors, which negates the need for motor drive shaft feedthroughs. This simplifies the mechanical design of the instrument and removes the heat load due to the drive shafts, although the work done by the cold motors now needs to be dissipated into the temperature sink (liquid nitrogen).

Formally, the power is given by:

$$P = 2\pi V\tau \text{ W} \quad (21)$$

where V is the motor velocity in revolutions/sec

τ is the motor torque in Nm

The standard motor for cryogenic applications in astronomical instruments is the Phytron VSS 52 motor (e.g. NIRI, GNIRS, NIFS, and IRCS). Figure 17 shows the speed versus drive torque and power for this motor. The actual power characteristic (red) is in reasonable agreement with Equation 21 (implying a motor efficiency of about 73%). At typical drive speeds of 300 rev/min (torque

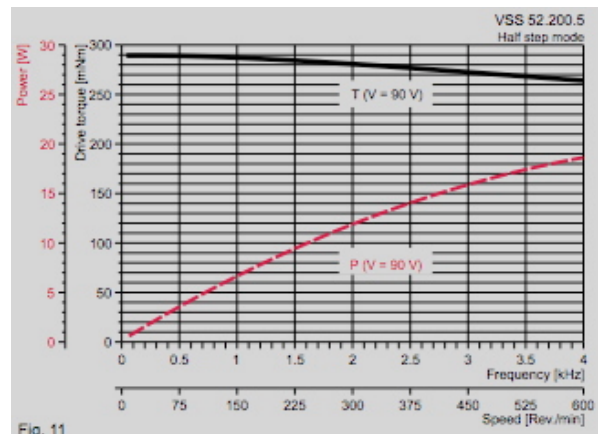


Figure 17. Speed vs drive torque and power for Phytron VSS 52.200.5 cryo-motor

120 mNm or 17 oz-in) the power dissipation is 12 W. Assuming five mechanisms are moved at this torque for one minute every hour for 12 hours per day, the average heat load is about 0.5 W.

Assuming a similar thermal mass to SpeX (140 Kg), iSHELL will require a similar support truss and therefore a similar heat load. Currently the entrance window is sized to accept a FOV of 60" x 60" (the same as SpeX) so that we have the option of feeding this FOV to an optical wavefront sensor through a same-sized exit window. Since it is unlikely that the optical feed will be used in the foreseeable future we will assume that just one window will be used and it will be stopped down to the maximum useful infrared FOV (42" diameter), although the instrument will be built to allow simple modification to output the larger FOV.

Precision temperature control of the two immersion gratings requires that the two gratings be sufficiently thermally isolated from the cold structure to allow temperature control without the need for large heat inputs. Since the cool down time gets longer with increased thermal isolation the required thermal impedance is a trade off between heat input and cooling rate.

Using Equations 18-20 the thermal time constant of the Silicon immersion gratings can be estimated. Each grating has a mass of about 0.2 Kg ($c_p=200 \text{ Jkg}^{-1}\text{K}^{-1}$, Touloukian *et al.*, in *Thermophysical Properties of Matter* 1970). At an operating temperature of 80 K and with an OFHC ($k=5.2 \times 10^2 \text{ Wm}^{-1}\text{K}^{-1}$) thermal link to the 74 K heat sink with the dimensions $A/L=1 \times 10^{-4}$ m, and assuming the Silicon grating is in good thermal contact with its mount (Silicon has a relatively high thermal conductivity), the time constant is about 13 minutes. Therefore it takes 13 minutes to cool from 80 K to 77.8 K ($2.2 \text{ K} = e^{-1} \Delta T_0$, $\Delta T_0=80 - 74 \text{ K}$), i.e. a cooling rate of about 0.17 K/min. Therefore the gratings will take 7 seconds to respond to temperature changes of 0.02 K, the required stability. With a 100 Ω heater this requires current regulation/stability at the level of 3mA. Since the cold bench is expected to change temperature by about 1 K over the period of a few days as the liquid nitrogen level changes, this level of temperature control appears to be conservative. With this configuration the heat flow required to maintain a temperature of 80.0 K is about 0.3 W for each grating.

The estimated total static heat load is 10.2 W (see Table 2).

Table 2. Estimated static heat loads on LN₂ sink

<i>Source</i>	<i>Heat load/W</i>
Active shield	0.4
Holes in active radiation shield	0.3
Windows (1)	0.8 (TBD)
(Fiberglass support truss)	(2.5)
Titanium support truss	5.0
Fiberglass neck tubes	0.0
Cold motors	~0.5 (TBC)
Wiring	2.5
Immersion grating (2) temp. control	~0.6 (TBC)
Gas conduction	<0.01
<i>Total</i>	10.2

With the estimated 12 l of LN₂ the cooling capacity is 536 W hr and so the predicted hold time is roughly 53 hours or about 2.2 days.

The 80 K to ≈30 K cabling is almost exactly the same as SpeX. Four 50 mm wide and 1 mm thick PVC ribbon cables each about 65 mm long and each containing 32 AWG 30 manganin wires (similar to constantan) going to the H2RG (spectrograph at 38 K) and two similar cables going to the Aladdin 2 (guider at 30 K). Consequently thermal control will also be very similar.